Optimization Scheme Based on High-Frequency Link Interconnection of Submodules

Jiaxun Teng, Xiaofeng Sun, *Member, IEEE*, Zemin Bu, Wei Zhao, and Xin Li

***Abstract*—Submodule (SM) capacitor voltage ripple and imbalance are inherent problems with conventional modular multilevel converter (MMC). In addition, the large size capacitance in SM reduces the power density of MMC, and the life defect of electrolytic capacitor also decreases reliability of the converter. This article proposes a modified switched-capacitors based MMC (SC-MMC) topology with ripple-power decoupling channels. Without relying on any closed-loop control, the natural elimination of SMs ripple-power and automatic balance of SMs voltage can be realized simultaneously, which greatly increase the power density and simplify the control design of system. In this article, the ripple characteristic of the conventional MMC and the constraint on capacitance are studied, and an SMs ripple-power decoupling method is analyzed. The power characteristics and impedance constraint analysis of the switched-capacitors are described in detail and the configuration assessments including volume, cost, and efficiency of the SC-MMC are also analyzed. Finally, a down-scaled experimental platform is built, and the experimental results verify the correctness and effectiveness of the proposed scheme.**

***Index Terms*—Modular multilevel converter (MMC), ripple-power decoupling, switched-capacitors, voltage self-equalization.**

I. Introduction

THE medium- and high-voltage direct current transmission technology based on voltage source converter was first proposed and it has become a hot spot of research and application for ac/dc bidirectional conversion [1], [2]. The early flexible dc power transmission technology also adopted the two-level converter structure [3].

For a medium and high voltage system, the scheme of switches connected in series for the two-level converter is not widely used due to the series voltage equalization problem of power semiconductor devices, there are high requirements for the consistency of power devices and drive circuits. In recent years, multilevel technology has developed rapidly, and high-power multilevel converter has been widely used in the field of medium and high voltage. The typical multilevel topologies include neutral point clamped (NPC), flying capacitor (FC), cascaded H bridges (CHB), and modular multilevel converter (MMC) [4]. NPC converters still need to use IGBTs in series in medium and high voltage applications. As the number of levels increases, the number of clamping diodes will increase significantly, so it is difficult to expand to higher level numbers [5]. FC converters have found less industrial penetration, mainly because higher switching frequency is necessary to keep the capacitors properly balanced, whether a self-balancing or a control-assisted balancing modulation method is used [6]. CHB and MMC adopt the form of full bridge or half bridge SM cascaded to improve the voltage level, which has the advantages of low switching frequency, good redundancy, and modular design. Both the two converters are fits for medium- and high-voltage applications as they are conducive to the redundant design of the system, and can facilitate system expansion and fault ride-crossing [7], [8]. However, MMC has a common dc bus, while the CHB not. This feature makes the MMC more suitable for medium- and high-voltage dc transmission [9], [10].

MMC is a hot topic of current research and related advanced modulation strategies [11], [12], modeling analysis [13], [14], failure redundancy strategies [15], [16], etc., are constantly being proposed. Although there is no large size electrolytic capacitor on the MMC dc bus, a large number of electrolytic capacitors are used in SMs to support the sufficient medium and high voltage and suppress the SM voltage fluctuation [17], [18]. The presence of large capacitor in MMC greatly reduces the power density, while electrolytic capacitor has the issue of short service life [19]–[21]. In high-power engineering applications such as medium- and high-voltage flexible dc power transmission, MMC is required to have the ability of long-term stable operation. Therefore, reducing the size of MMC capacitors is of great significance for the practical engineering application of MMC. At present, the main methods of solving this problem can be divided into two categories: software methods and hardware methods.

The software method is to inject common-mode voltage and high-frequency circulating current into MMC. A beat frequency power component is generated in MMC arm to offset the fundamental frequency ripple power [22]–[24]. Although this effectively reduces the SM voltage ripple, the current stress of power device will increase significantly. In order to solve the problem of the increasing current stress, injection methods with different common-mode voltages and circulating current have

Manuscript received December 15, 2020; revised March 4, 2021 and April 30, 2021; accepted June 8, 2021. Date of publication June 11, 2021; date of current version August 16, 2021. This work was supported in part by the Key Program of National Natural Science Foundation of Hebei Province under Grant E2021203162, in part by the Key Research and Development Program of Hebei Province under Grant 19214405D, and in part by the National Natural Science Foundation of China under Grant 51677162. Recommended for publication by Associate Editor D. M. Xu. *(Corresponding author: Xiaofeng Sun.)*

The authors are with the Key Laboratory of Power Electronics for Energy Conversion and Motor Drive of Hebei Province, Department of Electronics Engineering, Yanshan University, Qinhuangdao, Hebei 066004, China (e-mail: tengjiaxun@qq.com; sxf@ysu.edu.cn; 18335388105@163.com; zwysu@163.com; yddylixin@ysu.edu.cn).

Color versions of one or more figures in this article are available at https://doi.org/10.1109/TPEL.2021.3088514.

Digital Object Identifier 10.1109/TPEL.2021.3088514

been studied. The methods of injecting a square-wave common-mode voltage on the ac side and injecting a circulating current into the phase unit were proposed in [25] and [26] to suppress the low-frequency component of the SM capacitor voltage. In [27], a control strategy based on injection of sine waves or square waves into upper and lower arms respectively was proposed with a good ripple suppression effect being achieved. Although the above schemes can reduce the current stress somewhat, the difficulty of controlling the injection waveform also increases accordingly.

The hardware method of designing additional circuits is also used in the study of reducing the capacitance of MMC SMs. In [28], an MMC scheme of flying capacitor structure (FC-MMC) was proposed. The flying capacitors are used to connect the upper and lower arms to achieve power balance between the two arms. The proposed scheme can use the corresponding circulating current injection method without common-mode voltage. In [29] and [30], a buck-type active power filter circuit is added into MMC topology (APF-MMC) to suppress the capacitors voltage fluctuations and decrease the power loss, and the SM capacitor ripples can be reduced up to 50% of the original value.

Ripple suppression schemes that provide power channels between SMs have also been studied. This scheme is based on the phase difference of ripple voltage between SMs, which can compensate and cancel each other. The methods proposed at present are mainly divided into two categories. One is to provide power channels for the SMs between the upper and lower arms of the phase unit to realize the decoupling of odd frequency ripple power [31]–[33]. The other is to provide power channels for SMs between different phases, including adjacent arms in single MMC [34], [35] and dual MMC [36]. Since no injection method is required, there are neither common-mode voltage nor current stress issues. Compared with injection method, the proposed MMC significantly reduces the total capacitance, avoids common-mode voltage injection, and does not significantly increase the total cost and power consumption. The power channels in the above schemes adopt the DAB structure, and a closed-loop control method needs to be designed in each SM, which will increase the complexity of system control in the multimodule system.

In addition, all above methods to suppress the SM capacitor voltage ripple have a common premise, that is, SM capacitor voltage has been equalized through corresponding control. Therefore, in addition to the above ripple suppression scheme, another voltage equalization control strategy should be designed. Switched capacitor converters realize power transfer by controlling the charging and discharging of capacitors through switching devices, which can reduce the volume and weight of the converter system, contribute to the improvement of power density, and have the structural characteristics of high integration [37], [38]. Kawa *et al.* [39] proposed a switched-capacitors based voltage doubling topology based on electronic thyristors, which takes thyristor as an active switch and constructs a resonant switching transformation mode, thus creating conditions for high voltage gain, high power, and low cost, and broadening the application field of switched-capacitor. Chen *et al.* [40] proposed a boost resonant switched capacitor converter applied to offshore wind energy systems, which realizes the soft switching of all switches and diodes, and achieves a higher switching frequency to reduce the volume of the system.

In order to eliminate the voltage ripple of SM capacitor and realize the voltage equalization among all SM capacitors, this article proposes a modified switched-capacitors based MMC (SC-MMC) topology with ripple-power decoupling channels. Compared with conventional MMC and the existing methods, the topology scheme has the following characteristics:

1) The power density is greatly improved compared with the conventional MMC. The ripple power of SMs can be almost eliminated, and the size of SM capacitor is greatly reduced. And the cost and power loss of the proposed topology have not increased significantly.
2) It can realize the automatic balance of SMs voltage, and achieve the natural suppression of the second-order frequency circulating current in arms while eliminating the SMs ripple-power, simplifying the control of MMC.
3) Compared with other power-channel schemes, the switched-capacitors loop of the proposed topology can eliminate the ripple-power without any closed-loop control.

The proposed SC-MMC topology scheme will pay some price while achieving power density improvement and control simplification, including the cost and loss slightly increase caused by the addition of decoupling channels. In the analysis of this article, a detailed comparison is made between the proposed SC-MMC, conventional MMC, and several topologies with power-channel, including volume, cost, and power loss, etc. And after analysis and verification, the cost and power loss of the proposed topology have not increased significantly.

In the next section, the ripple properties of conventional MMC and the constraints of SM capacitance are described. In Section III, the decoupling methods of ripple-power, the SC-MMC topology, working characteristics, and impedance constraint of switched capacitors loop, as well as the new capacitance parameter are analyzed in detail. The configuration assessments of the proposed SC-MMC are presented in Section IV, including volume, cost, and control method, etc. In Sections V and VI, simulation and experimental verification of voltage fluctuation suppression and self-equalization characteristics of SM capacitance are presented. Section VII summarizes the proposed topology scheme.

II. Ripple Characteristic of Conventional MMC

The conventional three-phase MMC, shown in Fig. 1(a), consists of six arms, each of which is formed by N series-connected SMs and one arm inductor. The SM unit is usually composed of a half bridge and a capacitor in parallel, and there are two effective working states of the SM, namely the inserted state and the bypassed state. MMC adjusts the output voltage of the arm by controlling the state of each SM unit.

The equivalent model of the conventional MMC is shown in Fig. 1(b), where u_{x} and i_{x} are the ac side voltage and current, respectively (x stands for a, b or c); u_{ux}, u_{dx}, i_{ux}, and i_{dx} are the voltage and current of the upper and lower arms, respectively;

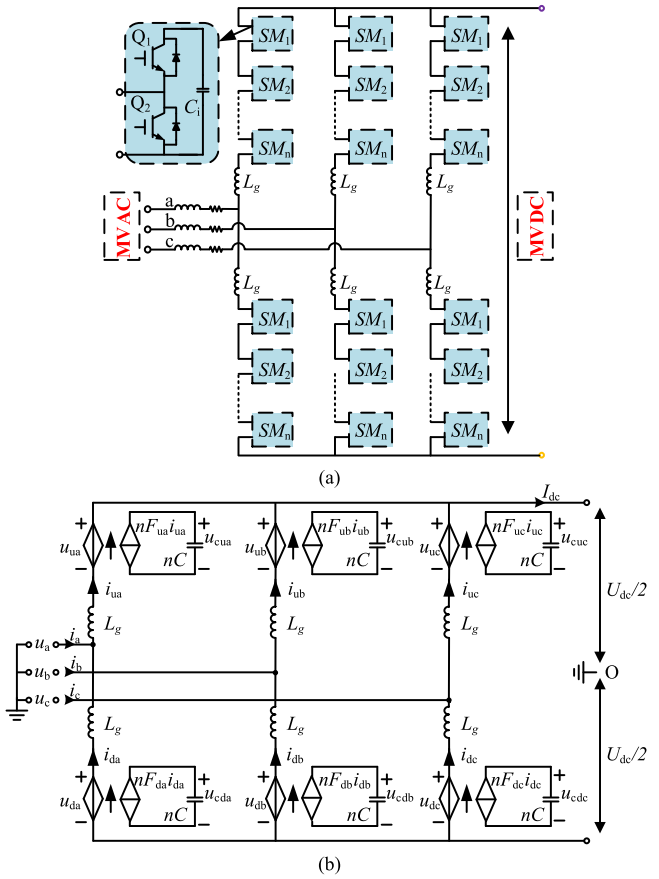

Fig. 1. Conventional MMC. (a) MMC topology. (b) MMC equivalent model diagram.

$F_{\rm ux}$ and $F_{\rm dx}$ are switch functions of upper and lower arms, respectively; $U_{\rm dc}$ and $I_{\rm dc}$ are dc voltage and current, respectively; L_g is the inductance of the phase arm. In order to facilitate the analysis of the ripple characteristics of MMC, it is assumed that the SMs have achieved voltage balance under corresponding control. Due to the imbalance between the three-phase dc voltages, negative-sequence interphase circulating current will be generated inside the MMC. The internal circulation of MMC is dominated by second-order harmonic component [8].

The voltage and current of the upper and lower arms in Fig. 1(b) are expressed as

$$\begin{cases} u_{\rm ux} = \frac{1}{2}U_{\rm dc} - U_{\rm x}\cos(\omega t + \theta_{\rm x}) \\ u_{\rm dx} = \frac{1}{2}U_{\rm dc} + U_{\rm x}\cos(\omega t + \theta_{\rm x}) \\ i_{\rm ux} = \frac{1}{3}I_{\rm dc} + \frac{1}{2}I_{\rm x}\cos(\omega t + \varphi + \theta_{\rm x}) + I_{2\rm x}\cos(2\omega t + \theta_{2\rm x}) \\ i_{\rm dx} = \frac{1}{3}I_{\rm dc} - \frac{1}{2}I_{\rm x}\cos(\omega t + \varphi + \theta_{\rm x}) + I_{2\rm x}\cos(2\omega t + \theta_{2\rm x}) \end{cases} \tag{1}$$

where $U_{\rm x}$ is the phase-x voltage amplitude of MMC; $I_{\rm x}$ is the amplitude of the phase-x current; $I_{2\rm x}$ is the amplitude of the second harmonic component of the MMC phase-to-phase circulating current; ω is the angular frequency of the grid; $\theta_{\rm x}$ is the initial phase angle of the phase-x; φ is the power factor angle; and $\theta_{2\rm x}$ is the initial phase angle of the second harmonic circulating current. According to the relationship of voltages between arms and dc bus and taking the phase-x as an example, the switch functions of upper and lower arms are as follows:

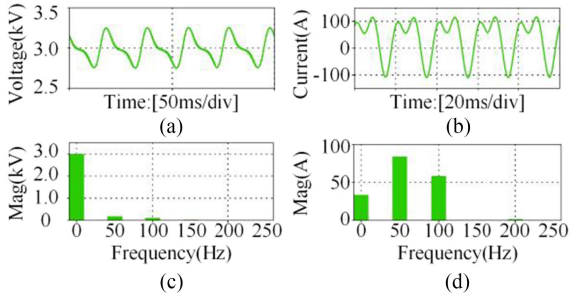

Fig. 2. Schematic diagram of fluctuation content of SM. (a) and (c) Voltage and FFT analysis of SM. (b) and (d) Current and FFT analysis of SM.

$$\begin{cases} F_{\rm ux} = \frac{u_{\rm ux}}{U_{\rm dc}} = \frac{1}{2}\left[1 - g\cos(\omega t + \theta_{\rm x})\right] \\ F_{\rm dx} = \frac{u_{\rm dx}}{U_{\rm dc}} = \frac{1}{2}\left[1 + g\cos(\omega t + \theta_{\rm x})\right] \end{cases} \tag{2}$$

where g is the voltage modulation ratio. From (1) and (2), the charging current of SM capacitor can be obtained

$$\begin{cases} C\frac{{\rm d}u_{\rm cux}}{{\rm d}t} = F_{\rm ux}i_{\rm ux} = i_{\rm ux\_dc} + i_{\rm ux\_ac} = i_{\rm x\_dc} + i_{\rm x\_f1} \\ \qquad\qquad +i_{\rm x\_f2} + i_{\rm x\_f3} \\ C\frac{{\rm d}u_{\rm cdx}}{{\rm d}t} = F_{\rm dx}i_{\rm dx} = i_{\rm dx\_dc} + i_{\rm dx\_ac} = i_{\rm x\_dc} - i_{\rm x\_f1} \\ \qquad\qquad +i_{\rm x\_f2} - i_{\rm x\_f3} \end{cases} \tag{3}$$

where

$$\begin{cases} i_{\rm x\_dc} = \frac{1}{6}I_{\rm dc} - \frac{1}{8}gI_{\rm x}\cos(\varphi) \\ i_{\rm x\_f1} = \frac{1}{4}I_{\rm x}\cos(\omega t + \varphi + \theta_{\rm x}) - \frac{1}{6}gI_{\rm dc}\cos(\omega t + \theta_{\rm x}) \\ \quad - \frac{1}{4}gI_{2\rm x}\cos(\omega t - \theta_{\rm x} + \theta_{2\rm x}) \\ i_{\rm x\_f2} = -\frac{1}{8}gI_{\rm x}\cos(2\omega t + \varphi + 2\theta_{\rm x}) + \frac{1}{2}I_{2\rm x}\cos(2\omega t + \theta_{2\rm x}) \\ i_{\rm x\_f3} = -\frac{1}{4}gI_{2\rm x}\cos(3\omega t + \theta_{\rm x} + \theta_{2\rm x}). \end{cases} \tag{4}$$

Fig. 2 shows the voltage and current waveforms of MMC SM and the corresponding FFT diagrams. From (3) and Fig. 2, it can be known that the capacitor voltage fluctuation of the SM includes the fundamental, second-order, and third-order harmonic components. The formula (3) shows that the SM capacitance C has a negative correlation with the voltage ripple, and the capacitance constraint in the conventional MMC can be obtained referring to the existing literature [41], [42]

$$C = \frac{1}{3}\frac{U_{\rm dc}I_{\rm dc}}{ng\omega\varepsilon {u_c}^2\cos(\varphi)}\left[1 - \left(\frac{g\cos(\varphi)}{2}\right)^2\right]^{3/2} \tag{5}$$

where $u_{\rm c}$ represents the average value of N SMs capacitor voltage and g represents the voltage fluctuating rate.

According to (5), the capacitance value of the SM is positively correlated with the transmitted power, and negatively correlated with the fluctuation rate of capacitor voltage, that is, the suppression of steady-state voltage fluctuation of the SM is mainly accomplished by capacitance. In medium- and high-voltage applications, the capacitance of the SM is in the range of millifarad.

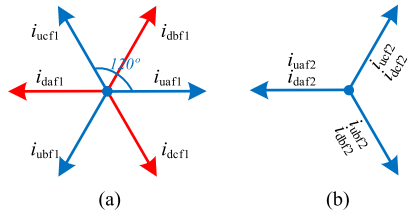

Fig. 3. Ripple components in six arms. (a) Fundamental frequency. (b) Second-order harmonic.

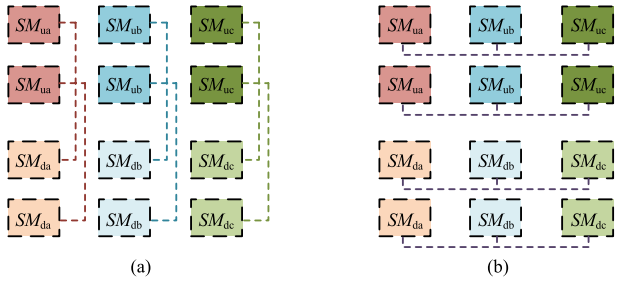

Fig. 4. SM ripple-power decoupling methods. (a) Vertical decoupling. (b) Horizontal decoupling.

In [43], the design process of a 2-MW experimental prototype was introduced in detail, in which the value of SM capacitance is 4.6 mF. Westerweller *et al.* [44] described the operation of a 400-MW power transmission project, and the SM capacitor design value is 7mF. Electrolytic capacitors are usually used, which makes the converter system bulky and heavy, and reduces the power density of system. And in actual projects that require long-term operation, the electrolyte inside electrolytic capacitor will cause chemical changes. Through long-term operation, the electrical parameters of electrolytic capacitors gradually deteriorate, reducing the reliability of system [14].

III. Improved MMC Based on Switched Capacitors

A. Analysis of SM Ripple-Power Decoupling

Under the assumption that the second-order harmonic circulating current has been suppressed ($I_{2x} = 0$), it can be seen from (3) and (4) that the input current of the SM includes the dc component and the ac component, and the ac part mainly includes fundamental and second-order harmonic components. Combined with Fig. 3, the following conclusions can be drawn:

1) For the SMs in one arm, all components of the ac current part have the same phase, and there are only differences in voltage amplitudes caused by imbalance between the SMs.
2) For the SMs between the upper and lower arms, the fundamental frequency components of the current ripple are in antiphase, while the second-order harmonic components have the same phase.
3) For the horizontal SMs, all components of the ac current part are three-phase symmetrical. The fundamental frequency components in horizontal SMs are in positive sequence, and the second-order harmonic components are in negative sequence.

From the phase relationship of ripple-power between different arms, two decoupling schemes as shown in Fig. 4 can be obtained. When the decoupling method as shown in Fig. 4(a) is adopted, it can be seen from the formula (6A) that the fundamental frequency components of the ripple current in the vertical SMs of the MMC cancel each other after decoupling, leaving second-order harmonic component. When using the decoupling method shown in Fig. 4(b), it can be seen from the (6B) that the ripple currents of the three-phase horizontal SMs compensate and cancel each other after decoupling because of their three-phase symmetry

$$i_{ux\_ac} + i_{dx\_ac} = 2i_{x\_f2} \tag{6A}$$

$$\begin{cases} i_{ua\_ac} + i_{ub\_ac} + i_{uc\_ac} = 0 \\ i_{da\_dc} + i_{db\_dc} + i_{dc\_dc} = 0. \end{cases} \tag{6B}$$

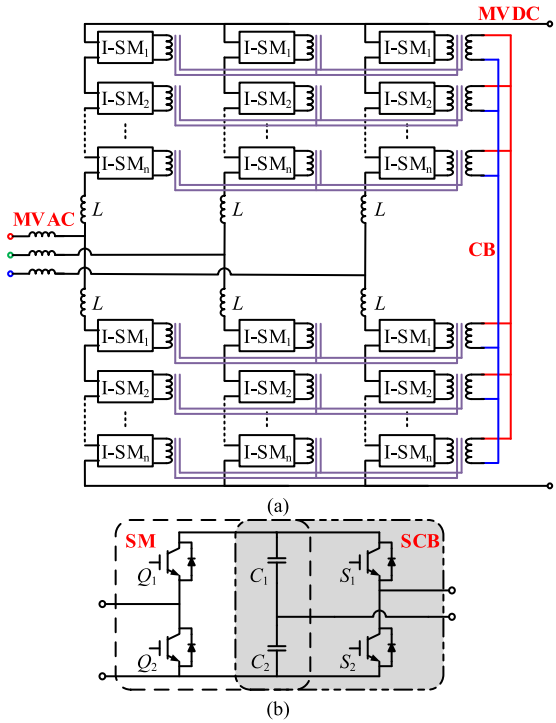

Fig. 5. Proposed SC-MMC. (a) SC-MMC topology. (b) Improved submodule.

B. Topology of SC-MMC

In view of the ripple characteristic of the conventional MMC and the defects caused by large size capacitor as analyzed in the previous section, as shown in Fig. 5(a), this article proposes a switched-capacitors based MMC topology with ripple-power decoupling channels, which can greatly reduce the size of SM capacitors. On the basis of the SM formed by the half-bridge parallel capacitor in the conventional MMC, the capacitor is disassembled into two capacitors in series, and the other half bridge is added to form a switched-capacitor bridge (SCB), constituting a new improved submodule (I-SM), as shown in

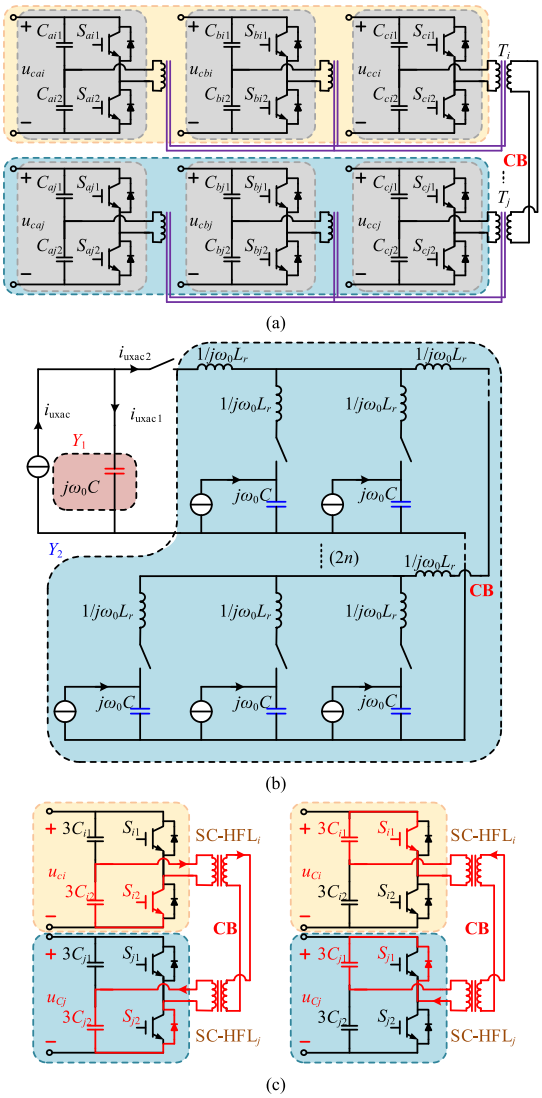

Fig. 6. Schematic diagram of switched-capacitors loop. (a) Switched-capacitors circuit. (b) Equivalent admittance model of I-SMs. (c) Voltage balancing process of capacitors.

Fig. 5(b). The windings on the primary side of transformer interconnect the horizontal three SMs of MMC, and the windings on the secondary side of all transformers are connected in parallel through a common bus (CB), providing power decoupling channels based on the switched-capacitor high-frequency link (SC-HFL) for all I-SMs of the three-phase six-arm MMC.

C. Analysis of the Switched Capacitors Based Ripple-Power Decoupling and Voltage Balancing of SMs

In order to replace the large size capacitor of the conventional MMC, an auxiliary circuit based on the SC-HFLs is introduced to the conventional SM as shown in Fig. 6(a). The SC-HFLs share the same drive signal source with fixed frequency and duty ratio, so the SMs can present the switched-capacitors characteristic. The auxiliary circuit can not only achieve the suppression of the ripple voltage, but also provide an active power transmission channel for the voltage imbalance between the SMs.

It can be known from (3) and Fig. 3 that the ripple currents in I-SMs are three-phase symmetrical. Therefore, if the ripple currents can flow freely between the three-phase SMs, they will cancel each other out, helping to eliminate the SM ripple-voltage (including the fundamental, second-order and third-order harmonic components). The elimination of the ripple-voltage in SMs means that there is no longer second-order frequency ripple in the single-phase dc voltage. Therefore, the second-order harmonic circulating currents caused by the ripple-voltage in negative sequence between the three phases is also eliminated. This helps to decrease the current stress of the power devices, at the same time reduces the loss caused by the circulating current.

Take one upper arm I-SM of phase-x as an example for analysis. An equivalent admittance model is established for describing the transfer of the ripple current i_{uxac}, as shown in Fig. 6(b). L_{r} is the inductance designed for the switched-capacitors loop, which is realized by the leakage inductance of transformer. The equivalent admittance can be obtained

$$\begin{cases} Y_1 = j\omega_0 C \\ Y_2 = \dfrac{j\omega_0 C[6n-1-(18n-1)\omega_0{}^2 L_{\mathrm{r}} C]}{24n(\omega_0{}^2 L_{\mathrm{r}} C)^2-(12n+1)\omega_0{}^2 L_{\mathrm{r}} C+1} \end{cases} \tag{7}$$

where Y_1 is the admittance of SM_1 without SC-HFL, Y_2 represents the equivalent admittance of the secondary side, and ω_0 is the equivalent angular frequency. From the equivalent admittance model, it can be obtained that the current ripple components of the SM flowing to its own capacitor and the secondary side are as follows:

$$\begin{cases} i_{\mathrm{uxac1}} = \dfrac{Y_1}{Y_1+Y_2} i_{\mathrm{uxac}} = \dfrac{24n(\omega_0{}^2 L_{\mathrm{r}} C)^2-(12n+1)\omega_0{}^2 L_{\mathrm{r}} C+1}{6n[4(\omega_0{}^2 L_{\mathrm{r}} C)^2-5\omega_0{}^2 L_{\mathrm{r}} C+1]} i_{\mathrm{uxac}} \\ i_{\mathrm{uxac2}} = \dfrac{Y_2}{Y_1+Y_2} i_{\mathrm{uxac}} = \dfrac{6n-1-(18n-1)\omega_0{}^2 L_{\mathrm{r}} C}{6n[4(\omega_0{}^2 L_{\mathrm{r}} C)^2-5\omega_0{}^2 L_{\mathrm{r}} C+1]} i_{\mathrm{uxac}}. \end{cases} \tag{8}$$

It can be seen from the above formula that when the leakage inductance is close to zero, the ripple current of SM will almost completely flow to the SC-HFL, and then cancel each other out. In the case that the SM voltage ripple has been significantly suppressed, the SC-HFL transferred power can be obtained as

$$\begin{aligned} p_{\mathrm{HFL}} &= u_{\mathrm{cux}} i_{\mathrm{uxac2}} \\ &\approx \frac{6n-1-(18n-1)\omega_0{}^2 L_{\mathrm{r}} C}{6n[4(\omega_0{}^2 L_{\mathrm{r}} C)^2-5\omega_0{}^2 L_{\mathrm{r}} C+1]} \frac{U_{\mathrm{dc}}}{n} i_{\mathrm{uxac}} \\ &= \frac{6n-1-(18n-1)\omega_0{}^2 L_{\mathrm{r}} C}{6n[4(\omega_0{}^2 L_{\mathrm{r}} C)^2-5\omega_0{}^2 L_{\mathrm{r}} C+1]} \frac{U_{\mathrm{dc}}}{n} \Bigg[-\frac{1}{6} g I_{\mathrm{dc}} \cos(\omega t+\theta_{\mathrm{x}}) \\ &\quad + \frac{1}{4} I_{\mathrm{x}} \cos(\omega t+\varphi+\theta_{\mathrm{x}}) - \frac{1}{4} g I_{2\mathrm{x}} \cos(\omega t-\theta_{\mathrm{x}}+\theta_{2\mathrm{x}}) \\ &\quad - \frac{1}{8} g I_{\mathrm{x}} \cos(2\omega t+\varphi+2\theta_{\mathrm{x}}) + \frac{1}{2} I_{2\mathrm{x}} \cos(2\omega t+\theta_{2\mathrm{x}}) \\ &\quad - \frac{1}{4} g I_{2\mathrm{x}} \cos(3\omega t+\theta_{\mathrm{x}}+\theta_{2\mathrm{x}}) \Bigg]. \end{aligned} \tag{9}$$

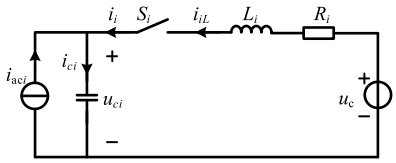

Fig. 7. Equivalent circuit of SC-HFL loop.

Due to the three-phase symmetry between the ripple power in the horizontal SMs, they cancel each other out, and due to the switching-capacitors characteristic, the horizontal three SMs voltages will be automatically balanced first. The imbalance of the capacitor voltage mainly occurs between the vertical SMs, which is addressed by the CB connecting SC-HFL units. In order to simplify the description process of voltage balance between vertical SMs, three horizontal SCBs are equivalent to one SCB, as shown in Fig. 6(c).

Any two SC-HFLs can be used to describe the capacitors voltage automatic balancing process between vertical SC-HFLs. Taking SC-HFL$_i$ and SC-HFL$_j$, for example, when the voltage of C_i is higher than C_j, that is, $u_{ci} > u_{cj}$, the energy path from C_i to C_j is shown in Fig. 6(c). The transformer turns ratio is 1: 1. When $u_{ci} > u_{cj}$, the current flows from C_i through the two SC-HFLs into C_j. SC-HFL$_i$ works in a square wave inversion mode, and SC-HFL$_j$ works in a rectification mode. The energy transfer ends when the two SC-HFLs have the same bus voltage. The whole process is carried out by SC-HFLs autonomously, without additional system control.

D. Impedance Constraint Analysis of Switched-Capacitors Loop

The realization of SC-MMC ripple-power elimination and voltage self-equalization functions relies on the autonomous flow of energy caused by the voltage difference between SMs. According to Fig. 6, while the switched-capacitors loop parameters difference is within the reasonable range, the equivalent circuit of SC-HFLs is obtained as shown in Fig. 7. u_{ci} is the capacitor voltage of SMi. u_c is the average voltage value of the SMs capacitors, and it can be drawn that $u_c \approx U_{\rm dc}/n$ in the case of minimal power loss. R_i is the equivalent resistance in the power channel including the ON-state resistance of diode and IGBT, as well as the resistance of high frequency transformer. L_i is the leakage inductance of the high-frequency transformer.

By applying the KVL theorem, it can be obtained within half a switching period

$$L_i \frac{di_i}{dt} + R_i i_i + u_{ci} = u_c \tag{10}$$

where

$$i_i = i_{ci} - i_{\rm aci} = C\frac{du_{ci}}{dt} - i_{\rm aci}. \tag{11}$$

The $i_{{\rm ac}i}$ is the input current of SM, which can be regarded as a constant during the switching period of SC-HFL. Substituting (11) into (10) yields

$$\frac{d^2u_{ci}}{dt^2} + \frac{R_i}{L_i}\frac{du_{ci}}{dt} + \frac{u_{ci}}{L_iC} = \frac{u_c + R_i i_{\rm aci}}{L_iC}. \tag{12}$$

The solution of (12) contains two parts: transient response $u_{\rm ci\_t}$ (t) and steady-state response $u_{\rm ci\_s}$ (t)

$$u_{ci}(t) = u_{ci\_t}(t) + u_{ci\_s}(t). \tag{13}$$

In order to simplify the solution process of transient response, the exponential form is adopted, and

$$u_{ci\_t}(t) = Ae^{st} \tag{14}$$

where A and s are constants, which can be obtained from the initial state parameters of the system. In the case of $u_c + R_i i_{{\rm ac}i} = 0$, substituting (14) into (12) yields

$$\frac{d^2Ae^{st}}{dt^2} + \frac{R_i}{L_i}\frac{dAe^{st}}{dt} + \frac{Ae^{st}}{CL_i} = 0. \tag{15}$$

Further solving, the following can be obtained:

$$Ae^{st}\left(s^2 + \frac{R_i}{L_i}s + \frac{1}{L_iC}\right) = 0. \tag{16}$$

Two solutions of the second-order system can be obtained

$$\begin{cases} s_1 = -\alpha + \sqrt{\alpha^2 - {\omega_{LC}}^2} \\ s_2 = -\alpha - \sqrt{\alpha^2 - {\omega_{LC}}^2} \end{cases} \tag{17}$$

where

$$\begin{cases} \alpha = R_i/2L_i \\ \omega_{LC} = 1/\sqrt{L_iC}. \end{cases} \tag{18}$$

It can be seen that there are two solutions in the transient response

$$u_{ci\_t}(t) = A_1e^{s_1t} + A_2e^{s_2t}. \tag{19}$$

In the SC-HFL loop, $R_{\rm i}$ is the equivalent circuit resistance, and its value is relatively small. Therefore, the loop works in an underdamped state, with $\alpha < \omega_{LC}$, that is, $C < 4L_{\rm i}/R_{\rm i}$. Equation roots can be obtained

$$\begin{cases} s_1 = -\alpha + j\omega_{\rm d} \\ s_2 = -\alpha - j\omega_{\rm d} \end{cases} \tag{20}$$

where $\omega_{\rm d} = \sqrt{({\omega_{LC}}^2\text{-}\alpha^2)}$, which is the damping frequency of SC-HFL loop. With the Euler Formula, (19) can be rewritten

$$u_{ci\_t}(t) = (B_1\cos\omega_d t + B_2\sin\omega_d t)\,e^{-\alpha t} \tag{21}$$

where $B_1 = A_1 + A_2$, $B_2 = A_1 - A_2$. The steady-state response $u_{\rm ci\_s}(t) = u_{\rm c} + R_i i_{{\rm ac}i}$ and the general solution of capacitor voltage can be obtained

$$u_{ci}(t) = (u_c + R_i i_{\rm aci}) + (B_1\cos\omega_d t + B_2\sin\omega_d t)\,e^{-\alpha t}. \tag{22}$$

The theoretical curves without considering the parameters of the I-SM is shown in Fig. 8. The charging and discharging current of C_i can be obtained from (11)

$$\begin{aligned} i_{ci}(t) = Ce^{-\alpha t}[&(-\alpha B_1 + B_2\omega_d)\cos\omega_d t \\ &- (\alpha B_2 + B_1\omega_d)\sin\omega_d t] \end{aligned} \tag{23}$$

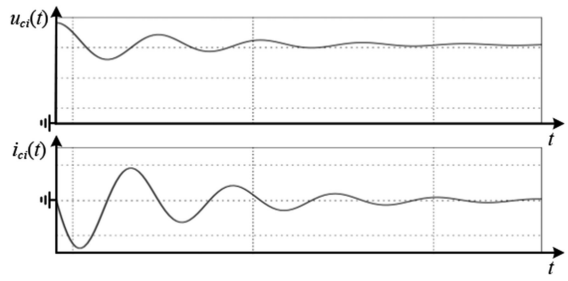

Fig. 8. Theoretical curves of switching capacitor.

where the time constant $\tau = 1/\alpha$, resonance period $T_{\rm d} = 2\pi/\omega_{\rm d}$, and then

$$\tau = \frac{2L_i}{R_i}, T_{\rm d} = \frac{\sqrt{C}L_i\pi}{\sqrt{4L_i - {R_i}^2 C}}. \tag{24}$$

In order to ensure the safety of voltage and current stress, it is necessary to analyze the corresponding parameter constraints. When $u_{ci} = (1\pm\varepsilon)u_c$, the attenuation characteristic of the exponential function shows that $|u_c$-$u_{ci}(t)|$ will be less than 1% of the initial value after five time-constant, and the following formula can be obtained:

$$\frac{L_i}{R_i} < \frac{1}{20f}. \tag{25}$$

When the switching frequency of SC-HFL changes, the leakage inductance parameter constraint of the high-frequency transformer satisfies (25), which can realize the fluctuating power natural elimination and voltage self-balancing of the SM capacitor. At the same time, the resonance period should be less than half of the switching period to ensure that there will be no large current peak when the switching state is switched, that is

$$\frac{2\sqrt{C}L_i\pi}{\sqrt{4L_i - {R_i}^2 C}} < \frac{1}{f}. \tag{26}$$

To find the maximum value of i_i(t), rewrite (23) as

$$i_{ci}(t) = Ce^{-\alpha t}\sqrt{(\alpha^2 + {\omega_d}^2)({B_1}^2 + {B_2}^2)}\sin(\omega_{\rm d}t + \arctan X) \tag{27}$$

where

$$X = \frac{\alpha B_2 + B_1\omega_{\rm d}}{\alpha B_1 - B_2\omega_{\rm d}}. \tag{28}$$

During the switching period, the capacitor voltage and leakage current in the switched-capacitors loop are shown in Fig. 8. The current peak will appear at the following moments:

$$t = \frac{\pi}{2\omega_{\rm d}} - \frac{\arctan X}{\omega_{\rm d}}. \tag{29}$$

At this time, the peak current can be obtained

$$i_{ci\_\max} = C\sqrt{(\alpha^2 + {\omega_d}^2)({B_1}^2 + {B_2}^2)}e^{-\alpha(\frac{\pi}{2\omega_{\rm d}} - \frac{\arctan X}{\omega_{\rm d}})} \tag{30}$$

where B_1 and B_2 can be obtained by $u_{\rm ci}(0)$ and $i_i(0)$, respectively, corresponding to the real-time SM capacitor voltage and input current.

E. Analysis of I-SM Capacitance Constraint

According to the above analysis, after the SCB transfers the ripple power in the SM to the SC-HFL, the capacitor $C_{\rm i}$ only deals with the high-frequency switching harmonics generated in SM. Since the SC-HFL switching frequency is much higher than SM, the switching harmonics absorbed by the capacitor are mainly determined by the switching frequency of SM half bridge. Considering that about 1/6*n* of the switching harmonic current generated in SM flows into $C_{\rm i}$, the $C_{\rm i}$ in each switching cycle of charging energy defined as $\Delta E_{\rm c}$, can be obtained

$$\Delta E_c = i_{\rm uxac1\_max} D_{\rm sm}/f_{\rm sm} \tag{31}$$

where $D_{\rm sm}$ is the duty cycle of the SM switching tubes, and its maximum value is equal to the voltage modulation ratio g, and the capacitor voltage ripple formed by $\Delta E_{\rm c}$ is

$$\varepsilon u_c = \frac{\Delta E_c}{C_i} = \frac{g i_{\rm uxac1\_max}}{C_i f_{\rm sm}}. \tag{32}$$

Ignoring the second-order harmonic circulating current $I_{2\rm x}$ in the system, the capacitance C_i of the SM in SC-MMC can be obtained from (3), (8), and (32)

$$C_i = \frac{I_{\rm dc}}{6\varepsilon U_{\rm dc} f_{\rm sm}}\left(-\frac{1}{6}g^2 - \frac{1}{2\cos\varphi}g + \frac{1}{\cos\varphi}\right). \tag{33}$$

IV. Assessment of the Proposed SC-MMC

A. Assessment of Volume and Cost

In terms of the number of system components and power density, referring to the comparison method of power density between conventional MMC and new MMC topologies in [45], this article compares the system volume from the aspects of switching devices, high-frequency magnetic components, and SM capacitors. In order to facilitate the device selection for an engineering application platform, under the premise that the overall structure of the research case remains unchanged, the power rate level is increased by 10 times on the basis of the simulation case, that is, the 12 kV/12 MW system is taken as an example for analysis. Since the number of SMs is the same in both topologies, the comparison contains only one SM.

For the selection of half-bridge switching devices in SM, 5SNA1200G450300 single-tube IGBT module with 4500 V/1200 A power rating is selected, and its unit volume is 1.28 dm^3 [46]. For the selection of half-bridge switching devices in SC-HFL, the 5SNA0650J450300 single-tube IGBT module of 4500V/650A is selected, and its unit volume is 0.87 dm^3 [47]. The above two models of IGBT are all from ABB. Therefore, the volume occupied by the switching device in the SM of the conventional MMC is 2.56 dm^3, and that in I-SM of proposed SC-MMC is 4.3 dm^3. The cost of IGBTs for the conventional MMC is 2589.2 USD and for the proposed SC-MMC, it is 4508.2 USD. The heat sink design matching the IGBT module is calculated referring to the research in [48]. The heat sink

volume of the conventional MMC SM is about 10.2 dm^3, and the required heat sink volume of the SC-MMC I-SM is about 17.2 dm^3.

The decoupling of I-SM ripple power in SC-MMC needs to be isolated. In the research case, a 3-kV/400-A high-frequency transformer needs to be designed in I-SM. Based on the existing research on the design of high-power and high-frequency transformers [49]–[51], this article calculates the volume of the component in this case, which is about 34 dm^3. Therefore, the volume of the magnetic components in each I-SM cell of the SC-MMC is approximately 11.3 dm^3, and the cost is about 2797.6 USD taking into account quotations from several manufacturers.

Taking ±5% capacitor voltage ripple as the standard, the capacitance value of SM in the 12 MW study case can be obtained from (5) and (33), the required capacitance in the conventional MMC is 7.2 mF, and in SC-MMC is 71 μF. In order to improve the power density of the system, electrolytic capacitors are usually used when selecting the SM capacitor types of conventional MMC [52]. Y. Zhang of Aalborg University proposed that the MMC engineering system has higher requirements for reliability and should seek to replace electrolytic capacitors with thin-film capacitors [53]. In order to evaluate the power density of the proposed topology more comprehensively, this article separately calculates the size of the SM using electrolytic capacitors and film capacitors.

When the conventional MMC adopts electrolytic capacitors (E-MMC), since the electrolytic capacitors have the limitation of lower rated working voltage, it is necessary to use multiple sets of capacitors in series and then parallel to meet the requirements of voltage and capacitance. In this article, the LNX2H123MSEK capacitor cell from Nichicon with 500 V/12 mF power rating is selected, which volume is 1.73 dm^3 [54]. Six capacitor units are connected in series to form a group, and then four groups are connected in parallel to form an SM capacitor. So when electrolytic capacitors are used, the capacitance volume of one SM of E-MMC is 41.5 dm^3, and the cost is 6731.7 USD. When the conventional MMC adopts film capacitors (F-MMC), TDK high-voltage capacitors with rated voltage of 3 kV and peak voltage of 4.5 kV are selected as the research object. In the conventional MMC, 18 capacitors B235680B3407K003 of 400 μF are required to be used in parallel, with a unit volume of 5.3 dm^3, so the total volume of capacitors in an SM of F-MMC is 95.4 dm^3, and the total cost is 4758.7 USD. In SC-MMC, choose two 3000 V/140 μF capacitors B25680B3147K003 with volume of 9.6 dm^3 [55] to form a capacitor half-bridge, which costs 164.8 USD. It can be seen that the reduction of SM capacitance greatly reduces the overall volume of the system, which is beneficial to the power density design of the system.

Fig. 9 shows the volume comparison result of the main components in one SM between the conventional MMC and SC-MMC. The result shows that the volume of SC-MMC is decreased by 26.5% compared to E-MMC, and 63.1% compared to F-MMC. Moreover, the contents in Fig. 9 are only the main components in SM (switching devices, heat sink, transformer, and SM capacitor), excluding the detection circuit, etc., and corresponding detection circuits should be configured for the

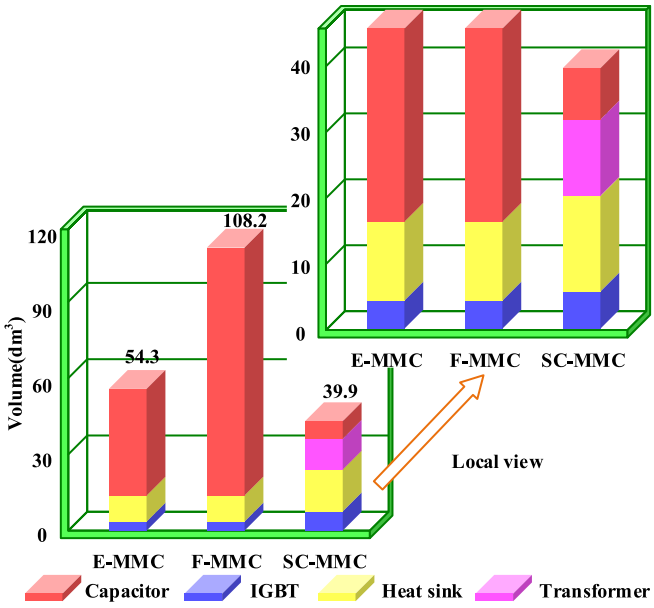

Fig. 9. Component volume comparison of SM both in conventional MMC and proposed SC-MMC.

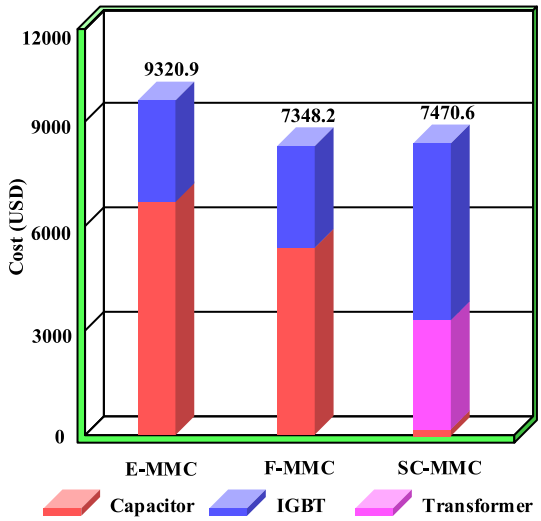

Fig. 10. Cost comparison of SM both in conventional MMC and proposed SC-MMC.

suppression of circulating current and the balanced control of capacitor voltage in the conventional MMC. The significant reduction in the volume of the main components would significantly increase the power density of the system design. At the same time, the cost of the I-SM has not risen obviously as shown in Fig. 10, and because high-voltage electrolytic capacitors are difficult to manufacture, the cost of the proposed SC-MMC has been reduced compared to E-MMC.

B. Combined Submodule Design

In order to further evaluate the practical engineering value of the proposed SC-MMC, this article proposes the system configuration structure as shown in Fig. 11. Three I-SMs in the same position of three phases are integrated to produce a new

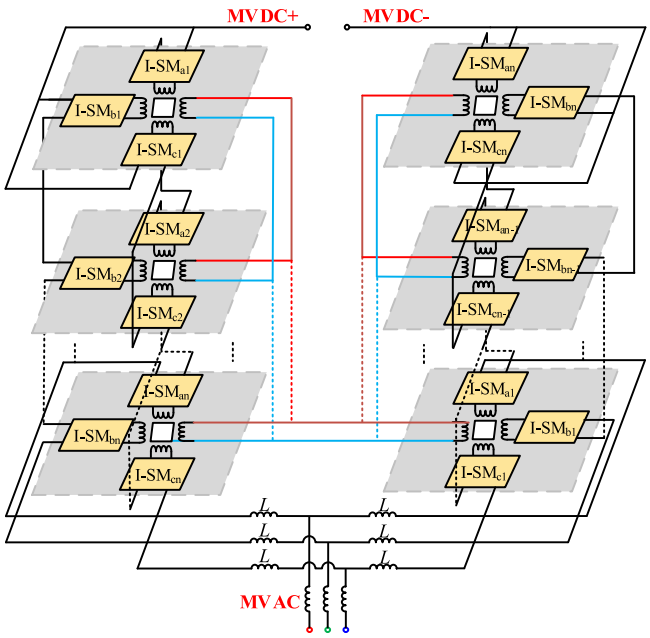

Fig. 11. Combined submodule design schematic.

combined submodule, as shown in the gray area in Fig. 11. The parasitic parameters of the high-frequency link in the combined structure are consistent, and the modularization degree is higher than that of the traditional three-phase parallel structure.

For the redundancy strategy of the proposed SC-MMC, the feature of only bypassing one fault SM does not remain, the asymmetric operation cannot be achieved for the proposed topology. When one SM is bypassed due to fault, so does the two SMs in the other two phases simultaneously to avoid the problem of asymmetrical three-phase operation, that is, a group SMs as a unit is bypassed, including the horizontal three SMs.

C. Comparison With Other Power Channel Methods

In order to highlight the characteristics of the proposed decoupling method of ripple-power based on the switched-capacitors structure, this article compares the SC-MMC topology with conventional MMC and several existing decoupling schemes [31], [33]–[35] in detail, and the results are shown in Table I.

The control of power decoupling channels is the most important difference between SC-MMC and existing schemes, that is, without relying on any closed-loop control, it realizes the free decoupling of ripple-power by designing the parameters of switched-capacitors loop under the simplest open-loop control with fixed frequency and duty ratio. At the same time, the added common bus makes all SMs clamped to each other, which brings the effect of SMs voltage automatic balance, while in conventional MMC and the existing power decoupling schemes, it is still necessary to design voltage balancing closed-loop control separately. Although the common bus brings some insulation problems, it can improve the security of the system by designing the corresponding fault response scheme. In the multimodule

TABLE I
CHARACTERISTICS COMPARISON BETWEEN PROPOSED METHOD AND OTHER METHODS

	MMC	[31]	[33]	[34]	[35]	SC-MMC
Ripple decoupling control loop	--	closed	closed	closed	closed	open
Low frequency SM ripple-voltage	all	even	even	none	none	none
SM voltage balancing control	yes	yes	yes	yes	yes	no
Number of SM switching tubes	2	4	4	4	6	4
Number of SM switching sensors	1	1	1	1	1	0
Number of Transformer	0	1/2	1/2	1/3	1	1/3

system, the open-loop control of SMs greatly saves the computing resource of the control center, reduces the cost, and improves the reliability of the control system.

In the conventional MMC, the voltage ripple components of the SM capacitor contain all low-frequency ac components. In the ripple-power decoupling schemes between upper and lower arms described in [31] and [33], there will be even frequency components left in the SM ripple voltage, and in the decoupling schemes proposed in [34] and [35] and this article, all ripple components will be completely eliminated theoretically. The power decoupling channel inevitably leads to the increase of components, mainly including switching tubes and magnetic components. Compared with the existing schemes, the number of components added in SC-MMC is still the least.

D. Comparison With Other Improved MMC Topologies

In order to further evaluate the value of the SC-MMC proposed in the study, this article compares the SC-MMC with two other existing improved MMC topology schemes, respectively, the FC-MMC proposed in [28] and APF-MMC in [29], mainly including volume and cost, efficiency, as well as control complexity.

From the perspective of components size and cost, FC-MMC does not provide an explanation of the reduction range of SM capacitor voltage fluctuations and the constraints of new capacitor parameters. The decoupling method of FC-MMC constructs power channels for the upper and lower arms. According to the principle of the formation of SM capacitor voltage fluctuations, the fundamental frequency component therein will cancel each other, and the capacitance value will be reduced to about 1/4 of the original value. In APF-MMC, the ripple power is suppressed by adding an APF to each phase unit, and the capacitance value is reduced by about 50%. The above two schemes can significantly reduce the volume and reduce the cost of the system without adding many components. Due to the addition of switching devices and high-frequency transformers, the cost of SC-MMC proposed in this article is slightly increased. But capacitance value of the SC-MMC proposed in this article can be reduced by two orders of magnitude, and the overall volume reduction

TABLE II
PARAMETERS OF MODEL 1 AND 2

MMC parameters		
Parameters	Model 1	Model 2
DC voltage/ U_{dc}	12kV	12kV
Line to line voltage/ U_{ac}	6kV	6kV
Rated active power / P	1.2MW	1.2MW
Fundamental AC frequency /f	50Hz	50Hz
PWM carrier frequency /f_c	2kHz	2kHz
Number of SMs per arm /n	4	4
SM equivalent capacitance /C	1200uF	10uF
Arm inductance /L	10mH	10mH
SC-HFL parameters		
Transformer turns ratio		4:4:4:1
Leakage inductance /L		9uH
Switching frequency /f_1		5kHz

is the most obvious compared with FC-MMC and APF-MMC, significantly increasing the power density of system.

From the perspective of efficiency, FC-MMC and APF-MMC can not only suppress the voltage fluctuation of SM capacitor, but also reduce the power loss of the second-order frequency circulation on the SM switch devices to a certain extent, which improves the overall efficiency of the system. The SC-MMC eliminates the second-order frequency circulating current of the arms while eliminating the SM voltage fluctuation, thus avoiding the power loss caused by it. However, the added power channel will bring the additional loss, thus reducing the overall system efficiency slightly. The efficiency data curve of SC-MMC is given in the experimental section.

From the perspective of control complexity, both FC-MMC and APF-MMC can suppress the arm circulating current to a certain extent, reducing the demand for its control strategies, but the SM voltage equalization control of the MMC is still required for the two topologies. The SC-MMC topology proposed in this article not only can realize the natural suppression of SM voltage fluctuations and arm circulating current, but also realize the automatic equalization of SMs voltage. The added power channel adopts the simplest fixed frequency and fixed duty cycle open-loop control, which significantly simplifies the control of MMC system.

V. SIMULATION VERIFICATION

A. Simulation Model

In order to verify the performance of the small size capacitor MMC with voltage self-equalization function proposed in this article, two sets of three-phase five-level MMC simulation models are built in the PLECS software. The simulation parameters of the models are shown in Table II.

Model 1: Three-phase five-level conventional MMC, half-bridge SM, using large-value electrolytic capacitors. The modulation method adopts carrier phase shift SPWM with voltage equalization control.

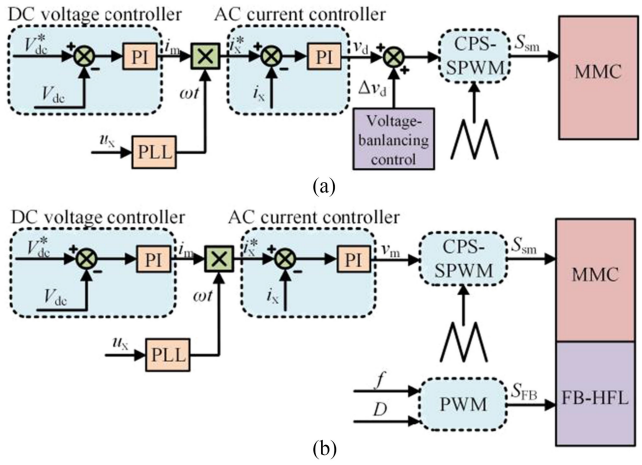

Fig. 12. Control block diagram. (a) Conventional MMC. (b) SC-MMC.

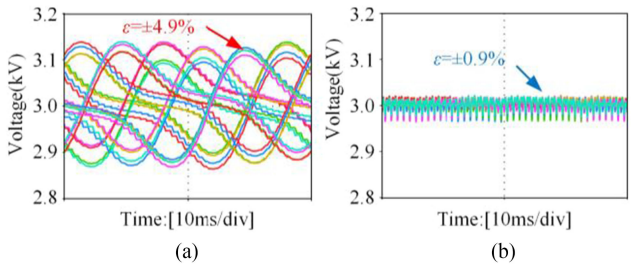

Fig. 13. Voltage waveforms of all SMs. (a) Model 1. (b) Model 2.

Model 2: Three-phase five-level SC-MMC, improved SM, using small-value thin film capacitors. The modulation method adopts carrier phase shift SPWM, without voltage equalization control.

The control schemes of Model 1 and 2 are shown in Fig. 12. The overall control methods of the two models are basically the same, and the difference is whether SM voltage balancing control is added.

B. Simulation Results

Figs. 13–15 show the comparison of simulation results of Model 1 and Model 2 under steady-state conditions. The simulation results in Fig. 13 show the good effect of Model 2 on SM voltage ripple suppression. In the conventional MMC topology of Model 1, the suppression of voltage fluctuation of SM capacitance depends on large size capacitance. In the SC-MMC topology of Model 2, the value of SM capacitance can be greatly reduced, and the use of thin-film capacitance can achieve a good ripple suppression effect. Fig. 14 is comparison diagram of the arm voltage simulation waveforms of Model 1 and Model 2, and it can be seen that the arm voltage in Model 2 is more symmetrical. Due to the existence of the power decoupling channel between SMs, most of the harmonic currents cancel each other after passing through the SC-HFL, so the arm voltage in Model 2 has less harmonic content. Fig. 15 is comparison diagram of the arm currents in Models 1 and 2, as well as the corresponding FFT results. It can be seen that Model 2

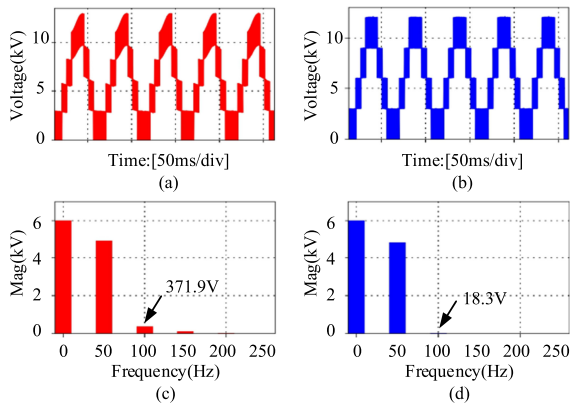

Fig. 14. Voltage simulation waveforms of upper and lower arms. (a) Model 1. (b) Mode 2.

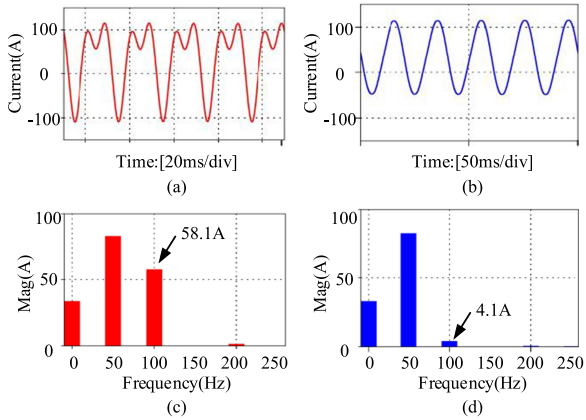

Fig. 15. Current waveforms and FFT analysis of phase arm. (a), (c) Model 1. (b), (d) Model 2.

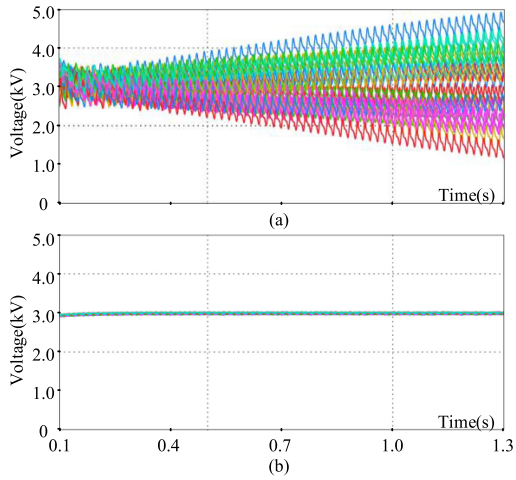

Fig. 16. Capacitor voltage waveforms of Model 1 without balancing control in (a) Model 1 and (b) Model 2.

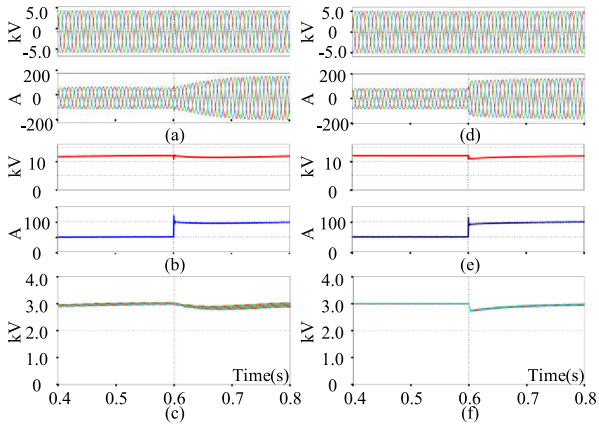

Fig. 17. Comparison of dynamic response capability when load is doubled. (a)–(c) MMC: Voltage and current at HVac side, voltage, and current at HVdc side, and voltage of SM. (d)–(f) SC-MMC: voltage and current at HVac side, voltage, and current at HVdc side and voltage of SM.

has an obvious inhibitory effect on the second-order harmonic current in the arm. According to the analysis in Section II, the second-order harmonic current component in bridge arm is formed by the three-phase negative sequence voltage of MMC, which will increase the switching loss and ON-state loss of the arm switching devices. The proposed SC-MMC effectively inhibits the generation of second-order circulating current in arms, and this is good for improving the efficiency of system.

According to the analysis in Section III, it can be seen that SC-MMC topology has SM voltage self-equalization characteristic. In order to verify its function, simulation analysis is carried out for Model 1 and Model 2 without voltage balancing control, and balanced factors (such as the inconsistency of capacitance parameters) are added to the model. The simulation results are shown in Fig. 16. Under the premise of no balancing control in Model 1, SM voltages show a divergent state. Model 2 has good SM voltage self-equalization characteristic without balancing control.

Fig. 17 shows the simulation results of Model 1 and 2 under the dynamic condition. It can be seen that due to the small capacitance used in Model 2, the response speed of the converter system is faster when the operating condition is suddenly changed. Therefore, the SC-MMC topology scheme has better dynamic performance.

VI. Experimental Verification

A. Experimental Results

In order to further verify the performance of the proposed SC-MMC topology, this article builds a down-scaled experimental platform. The photograph of the experimental platform is shown in Fig. 18. Since the ripple power decoupling scheme proposed in this article is applicable to MMC structures with any number of SMs, this article verifies the SC-MMC structure with one SM structure experimentally. TMS320F28335 from Texas Instruments is used in this platform, and the platform parameters are shown in Table III. The capacitance of the SM is a thin-film capacitor with the value of 9.4 μF.

Fig. 19 shows the working waveforms of the high-frequency transformer in horizontal I-SMs. SC-HFLs adopt the open-loop drive signals with the same switching sequence and frequency,

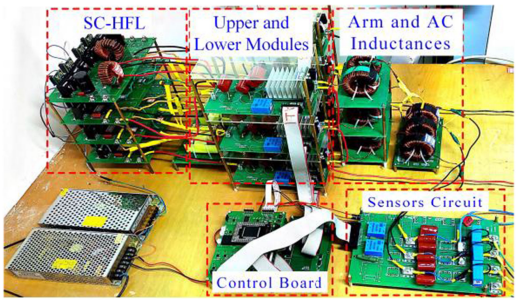

Fig. 18. Experimental prototype of the proposed SC-MMC.

TABLE III
PARAMETERS OF EXPERIMENTAL PLATFORM

MMC parameters	
Parameters	Value
Rated active power /	1.2kW
DC voltage/ U_{dc}	240V
AC current/ I_{ac}	5.6A
SM equivalent capacitance /C	9.4uF
SM capacitance voltage /u_c	240V
Fundamental AC frequency /f	50Hz
PWM carrier frequency /f_c	2kHz
Arm inductance /L	1.2mH
SC-HFL parameters	
Transformer turns ratio	2:2:2:1
Leakage inductance /L_r	4.3uH
Switching frequency /f_1	20kHz

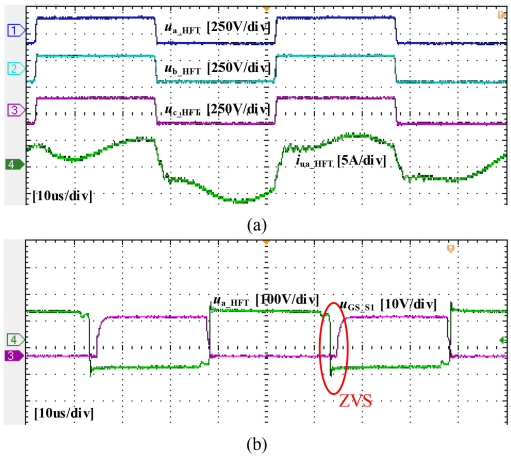

Fig. 19. Operating waveforms of SC-HFL. (a) Experimental waveforms of high frequency transformer. (b) ZVS of switches in SC-HFL.

so that the ripple-power can be transmitted freely among three I-SMs to achieve the purpose of mutual decoupling and cancellation. Fig. 19(b) shows that the switching devices in SC-HFL have good ZVS characteristic. When the voltage of the vertical SMs is imbalanced, according to the analysis in Section III-C, it can be known that the CB will transmit active power to realize the automatic balance of the SMs voltage, as shown in Fig. 20.

As shown in Fig. 21, the SC-HFL input current waveforms under steady-state operation verify the ripple characteristics and the ripple power decoupling analysis in Section III-A. If the ripple-power decoupling method in Fig. 4(b) is used,

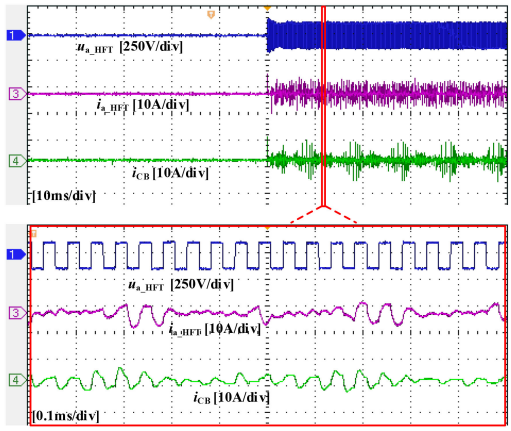

Fig. 20. Experimental waveforms of high frequency transformer and common bus before and after SC-HFL is connected.

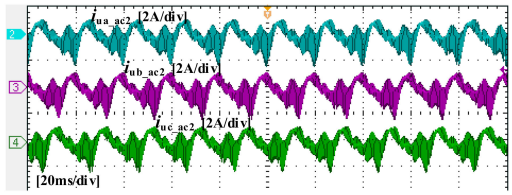

Fig. 21. Input current of horizontal SCBs.

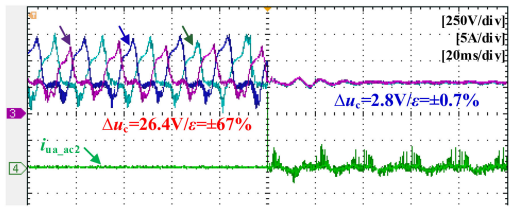

Fig. 22. SM capacitor voltages before and after SC-HFL is connected.

the horizontal SC-HFL input currents $i_{\mathrm{ua\_ac2}}$, $i_{\mathrm{ub\_ac2}}$, and $i_{\mathrm{uc\_ac2}}$ will all be coupled after isolation. The fundamental and second-order harmonic components in the ripple current are both three-phase symmetrical, and will completely be cancelled out after decoupling. Therefore, the capacitor in I-SM will no longer assume the task of suppressing voltage fluctuations.

Fig. 22 shows the experimental waveforms of capacitor voltage of SM. When the capacitor is 9.4 μF and the system is working at rated power without the SC-HFL, the ripple rate of SMs capacitors voltage is about 67%. The voltage difference between the three-phase horizontal SMs is 26.4 V, and the voltage deviation rate is 11%. When the SC-HFL is connected, Fig. 22 shows that the ripple current that produces voltage ripple on the SM capacitor is transferred to the secondary side, and after the mutual decoupling of horizontal SMs ripple-power, the capacitor voltage ripple is only ±0.7%. Moreover, the voltage imbalance of SMs is only 2.8 V. Experimental results show that the SC-MMC topology scheme has a good performance on suppressing SM capacitor voltage ripple, and it can also realize the voltage self-equalization among all SMs.

Fig. 23 shows the current waveforms of the upper and lower arms in phase-A. It can be seen that while suppressing the

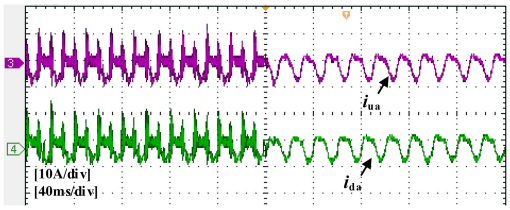

Fig. 23. Arm currents of phase-A before and after SC-HFL is connected.

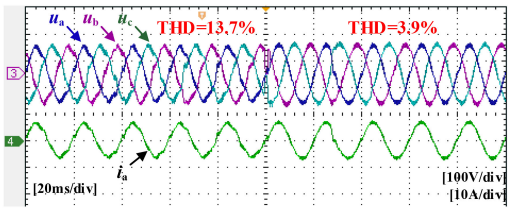

Fig. 24. Voltage and current waveforms at HVac side before and after SC-HFL is connected.

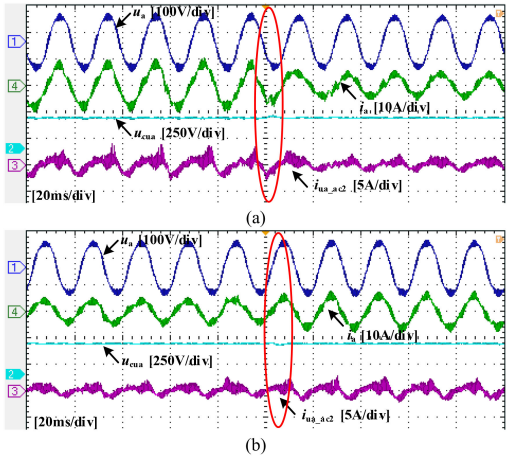

Fig. 25. Dynamic experimental waveforms in grid-connected state when power switches (a) from 100% to 50% and (b) from 50% to 75%.

SM capacitor voltage ripple, the SC-MMC topology effectively eliminates the second-order harmonic circulating current of MMC phase arm. Fig. 24 shows the experimental waveforms of SC-MMC on the ac side. With the help of the SC-HFL, the voltage ripple of the AC side is reduced to as the same as the capacitor voltage fluctuation. Moreover, the harmonic current content is eliminated somewhat by decoupling with each other between interconnection SMs, so the harmonic in the ac side is correspondingly decreased.

The waveforms shown in Figs. 25–27 are the dynamic experimental results, including the power switching process in the grid-connected state, the voltage jump process at the ac and dc sides. Fig. 25 shows that when the grid-connected power is switched between 100%, 50%, and 75%, the submodule capacitor voltage change is almost negligible, indicating that the ripple-power decoupling process between SMs is not disturbed. Figs. 26 and 27 show that when the ac and dc port voltage jumps, the ripple-power decoupling process is also not affected. The experimental results show that the ripple-power decoupling scheme has good performance in the dynamic process.

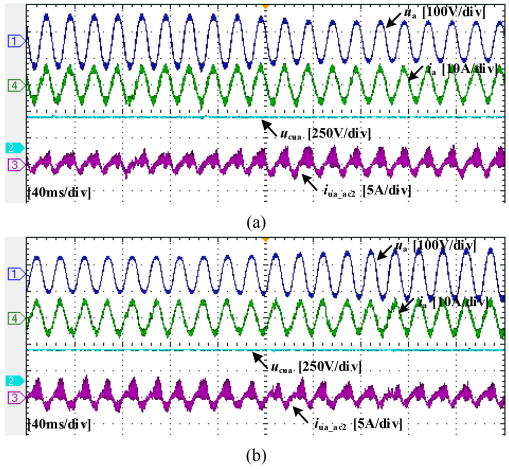

Fig. 26. Dynamic experimental waveforms when the ac grid voltage (a) sags by 20% and (b) swells by 20%.

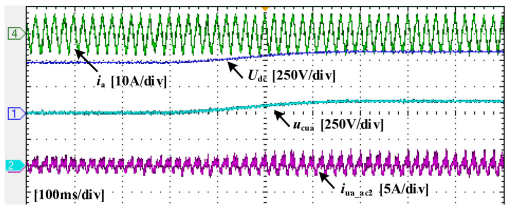

Fig. 27. Dynamic experimental waveforms when dc voltage swells by 20%.

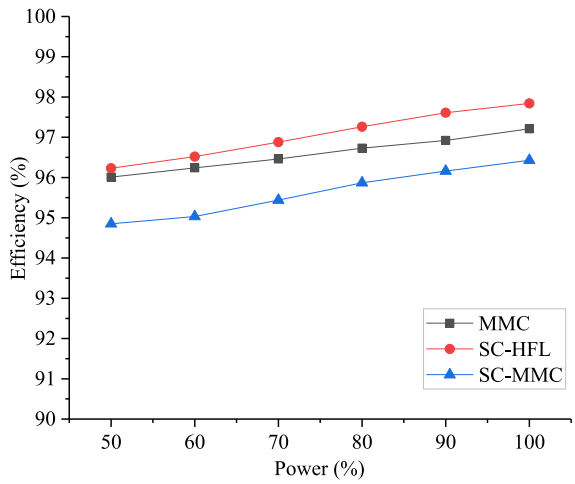

Fig. 28. Efficiency plots of hardware prototype.

B. *Efficiency Comparison*

The power decoupling channel added in SC-MMC will inevitably bring additional power loss, but it will also reduce the switching loss and ON-state loss caused by the second-order frequency circulating current of the bridge arms. And the significant reduction of SM capacitance will also reduce the capacitor loss accordingly. Huang *et al.* [34] gave an efficiency comparison between the injection and power channel methods, which are 96.77% and 96.86%, respectively, and there is no obvious difference between the two methods.

In the experiment process of this article, the efficiency data of the conventional MMC and proposed SC-MMC were tested,

respectively, and the efficiency of SC-HFL was tested separately. The plots are shown in Fig. 28. In the SC-HFL operating mode designed in this article, the switching devices of the power decoupling channel can realize zero-voltage switching (ZVS), thus reducing the switching loss of the decoupling loop. From (15), the proportion of SC-HFL processing power to the total system power can be estimated, and then the additional power loss of the power channel can be calculated, which is consistent with the total system power loss shown in Fig. 28.

VII. Conclusion

In this article, a modified switched-capacitors based MMC (SC-MMC) topology with ripple-power decoupling channels has been proposed to realize the cancellation of ripple-power. The ripple characteristic of the conventional MMC and the constraint characteristic of SM capacitance has been analyzed. The proposed SC-MMC topology, the power characteristics of the switched-capacitors, the impedance design of the switched-capacitors circuit-loop are described in detail, and the configuration assessments including volume, cost, and power loss of the SC-MMC are also analyzed. Compared with the conventional MMC, the proposed SC-MMC has main advantages in the following aspects.

1) The power density is greatly improved compared with the conventional MMC. The ripple-power of SMs can be almost completely eliminated, and the size of SM capacitor is greatly reduced.
2) It can realize the automatic balance of SMs voltage, and achieve the natural suppression of the second-order frequency circulating current in arms while eliminating the SMs ripple-power, implying the control of MMC system.
3) Compared with other power-channel schemes, the SC loop of the proposed topology can eliminate the ripple-power without any closed-loop control.

References

[1] B. T. Ooi and X. Wang, "Voltage angle lock loop control of the boost type PWM converter for HVDC application," *IEEE Trans. Power Electron.*, vol. 5, no. 2, pp. 229–235, Apr. 1990.

[2] B. T. Ooi and X. Wang, "Boost-type PWM HVDC transmission system," *IEEE Trans. Power Del.*, vol. 6, no. 4, pp. 1557–1563, Oct. 1991.

[3] Y. Zhang, G. P. Adam, T. C. Lim, S. J. Finney, and B. W. Williams, "Voltage source converter in high voltage applications: Multilevel versus two-level converters," in *Proc. IET Int. Conf. AC DC Power Transmiss.*, London, U.K., 2010, pp. 1–5.

[4] S. Kouro *et al.*, "Recent advances and industrial applications of multilevel converters," *IEEE Trans. Ind. Electron.*, vol. 57, no. 8, pp. 2553–2580, Aug. 2010.

[5] A. Marzoughi, R. Burgos, D. Boroyevich, and Y. Xue, "Design and comparison of cascaded H-Bridge, modular multilevel converter, and 5-L active neutral point clamped topologies for motor drive applications," *IEEE Trans. Ind. Appl.*, vol. 54, no. 2, pp. 1404–1413, Mar./Apr. 2018.

[6] J. Rodríguez, S. Bernet, B. Wu, J. O. Pontt, and S. Kouro, "Multilevel voltage-source-converter topologies for industrial medium-voltage drives," *IEEE Trans. Ind. Electron.*, vol. 54, no. 6, pp. 2930–2945, Dec. 2007.

[7] S. Rivera, S. Kouro, B. Wu, J. I. Leon, J. Rodríguez, and L. G. Franquelo, "Cascaded H-bridge multilevel converter multistring topology for large scale photovoltaic systems," in *Proc. IEEE Int. Symp. Ind. Electron.*, Gdansk, Poland, 2011, pp. 1837–1844.

[8] C. Tu, F. Xiao, Z. Lan, Q. Guo, and Z. Shuai, "Analysis and control of a novel modular-based energy router for DC microgrid cluster," *IEEE J. Emerg. Sel. Topics Power Electron.*, vol. 7, no. 1, pp. 331–342, Mar. 2019.

[9] A. Lesnicar, J. Hildinger, and R. Marquardt, "Modulares stromrichterkonzept für netzkupplungsanwendungen bei hohen spannungen," *ETG*, Herzogenaurach, Germany, 2002.

[10] H. Zhang, L. Jing, X. Wu, J. Jiang, H. R. Wickramasinghe, and G. Konstantinou, "Power flow control scheme for multiport power electronics transformers," *High Volt.*, vol. 3, no. 4, pp. 255–262, 2018.

[11] J. Lamb and B. Mirafzal, "An adaptive SPWM technique for cascaded multilevel converters with time-variant DC sources," *IEEE Trans. Ind. Appl.*, vol. 52, no. 5, pp. 4146–4155, Sep./Oct. 2016.

[12] S. Fan, K. Zhang, J. Xiong, and Y. Xue, "An improved control system for modular multilevel converters with new modulation strategy and voltage balancing control," *IEEE Trans. Power Electron.*, vol. 30, no. 1, pp. 358–371, Jan. 2015.

[13] N. Trinh, M. Zeller, K. Wuerflinger, and I. Erlich, "Generic model of MMC-VSC-HVDC for interaction study with AC power system," *IEEE Trans. Power Syst.*, vol. 31, no. 1, pp. 27–34, Jan. 2016.

[14] N. Rashidi, R. Burgos, C. Roy, and D. Boroyevich, "On the modeling and design of modular multilevel converters with parametric and model-form uncertainty quantification," *IEEE Trans. Power Electron.*, vol. 35, no. 10, pp. 10168–10179, Oct. 2020.

[15] J. Lamb and B. Mirafzal, "Open-circuit IGBT fault detection and location isolation for cascaded multilevel converters," *IEEE Trans. Ind. Electron.*, vol. 64, no. 6, pp. 4846–4856, Jun. 2017.

[16] H. Iman-Eini and M. Liserre, "DC fault current blocking with the coordination of half-bridge MMC and the hybrid DC breaker," *IEEE Trans. Ind. Electron.*, vol. 67, no. 7, pp. 5503–5514, Jul. 2020.

[17] P. Hu, R. Teodorescu, S. Wang, S. Li, and J. M. Guerrero, "A currentless sorting and selection-based capacitor-voltage-balancing method for modular multilevel converters," *IEEE Trans. Power Electron.*, vol. 34, no. 2, pp. 1022–1025, Feb. 2019.

[18] Q. Song, W. Liu, X. Li, H. Rao, S. Xu, and L. Li, "A steady-state analysis method for a modular multilevel converter," *IEEE Trans. Power Electron.*, vol. 28, no. 8, pp. 3702–3713, Aug. 2013.

[19] X. Sun, J. Teng, L. Qi, Y. Pan, Z. Bu, and M. Zhang, "Research on triple-Port MMC-based PET scheme based on high frequency links interconnection of horizontal sub-modules," in *Proc. IEEE 9th Int. Power Electron. Motion Control Conf.*, 2020, pp. 2061–2067.

[20] A. Ristow, M. Begović, A. Pregelj, and A. Rohatgi, "Development of a methodology for improving photovoltaic inverter reliability," *IEEE Trans. Ind. Electron.*, vol. 55, no. 7, pp. 2581–2592, Jul. 2008.

[21] X. Sun, J. Teng, Z. Bu, Y. Pan, W. Zhao, and X. Li, "Research on triple-port SST scheme based on the natural elimination of MMC sub-modules voltage fluctuation and imbalance," *IEEE J. Emerg. Sel. Topics Power Electron.,* to be published, doi: 10.1109/JESTPE.2021.3065235

[22] M. Hagiwara, K. Nishimura, and H. Akagi, "A medium-voltage motor drive with a modular multilevel PWM inverter," *IEEE Trans. Power Electron.*, vol. 25, no. 7, pp. 1786–1799, Jul. 2010.

[23] K. Wang, Y. Li, Z. Zheng, and L. Xu, "Voltage balancing and fluctuation-suppression methods of floating capacitors in a new modular multilevel converter," *IEEE Trans. Ind. Electron.*, vol. 60, no. 5, pp. 1943–1954, May 2013.

[24] J. Kolb, F. Kammerer, M. Gommeringer, and M. Braun, "Cascaded control system of the modular multilevel converter for feeding variable-speed drives," *IEEE Trans. Power Electron.*, vol. 30, no. 1, pp. 349–357, Jan. 2015.

[25] S. Debnath, J. Qin, and M. Saeedifard, "Control and stability analysis of modular multilevel converter under low-frequency operation," *IEEE Trans. Ind. Electron.*, vol. 62, no. 9, pp. 5329–5339, Sep. 2015.

[26] M. Hagiwara, I. Hasegawa, and H. Akagi, "Start-up and low-speed operation of an electric motor driven by a modular multilevel cascade inverter," *IEEE Trans. Ind. Appl.*, vol. 49, no. 4, pp. 1556–1565, Jul./Aug. 2013.

[27] J.-J. Jung, H.-J. Lee, and S.-K. Sul, "Control strategy for improved dynamic performance of variable-speed drives with modular multilevel converter," *IEEE J. Emerg. Sel. Topics Power Electron.*, vol. 3, no. 2, pp. 371–380, Jun. 2015.

[28] S. Du, B. Wu, N. R. Zargari, and Z. Cheng, "A flying-capacitor modular multilevel converter for medium-voltage motor drive," *IEEE Trans. Power Electron.*, vol. 32, no. 3, pp. 2081–2089, Mar. 2017.

[29] G. Jia, M. Chen, S. Tang, C. Zhang, and G. Zhu, "Active power decoupling for a modified modular multilevel converter to decrease submodule capacitor voltage ripples and power losses," *IEEE Trans. Power Electron.*, vol. 36, no. 3, pp. 2835–2851, Mar. 2021.

[30] G. Jia, M. Chen, S. Tang, C. Zhang, and B. Zhao, "A modular multilevel converter with active power filter for submodule capacitor voltage ripples and power losses reduction," *IEEE Trans. Power Electron.*, vol. 35, no. 11, pp. 11401–11417, Nov. 2020.

[31] L. He, K. Zhang, J. Xiong, S. Fan, X. Chen, and Y. Xue, "New modular multilevel converter with power channels between upper- and lower arms suitable for MV drives," in *Proc. IEEE Appl. Power Electron. Conf. Expo.*, Charlotte, 2015, pp. 799–805.
[32] A. Elserougi, A. Massoud, and S. Ahmed, "An h-bridge modular DC-DC converter with bidirectional flyback-based energy equalization modules," in *Proc. Int. Conf. Elect. Power Energy Convers. Syst.*, Kitakyushu, Japan, 2018, pp. 1–5.
[33] M. Sleiman, M. Koteich, H. F. Blanchette, H. Kanaan, and K. Al-Haddad, "Energy equalization module for modular multilevel converters in variable speed motor drives," in *Proc. 3rd Int. Conf. Renewable Energies Develop. Countries*, Zouk Mosbeh, Lebanon, 2016, pp. 1–6.
[34] X. Huang, Z. Wang, Z. Kong, J. Xiong, and K. Zhang, "Modular multilevel converter with three-port power channels for medium-voltage drives," *IEEE J. Emerg. Sel. Topics Power Electron.*, vol. 6, no. 3, pp. 1495–1507, Sep. 2018.
[35] M. S. Diab, A. M. Massoud, S. Ahmed, and B. W. Williams, "A modular multilevel converter with ripple-power decoupling channels for three-phase MV adjustable-speed drives," *IEEE Trans. Power Electron.*, vol. 34, no. 5, pp. 4048–4063, May 2019.
[36] M. S. Diab, A. M. Massoud, S. Ahmed, and B. W. Williams, "A dual modular multilevel converter with high-frequency magnetic links between submodules for MV open-end stator winding machine drives," *IEEE Trans. Power Electron.*, vol. 33, no. 6, pp. 5142–5159, Jun. 2018.
[37] J. Han, A. von Jouanne, and G. C. Temes, "A new approach to reducing output ripple in switched-capacitor-based step-down DC–DC converters," *IEEE Trans. Power Electron.*, vol. 21, no. 6, pp. 1548–1555, Nov. 2006.
[38] A. Ruderman, "Filter capacitance reduction in DC/DC step-down reconfigurable switched-capacitor converters by a balanced switching," in *Proc. 13th Int. Conf. Optim. Elect. Electron. Equip.*, Brasov, Romania, 2012, pp. 776–782.
[39] A. Kawa, R. Stala, A. Mondzik, S. Pirog, and A. Penczek, "High-power thyristor-based DC–DC switched-capacitor voltage multipliers: Basic concept and novel derived topology with reduced number of switches," *IEEE Trans. Power Electron.*, vol. 31, no. 10, pp. 6797–6813, Oct. 2016.
[40] W. Chen, A. Q. Huang, C. Li, G. Wang, and W. Gu, "Analysis and comparison of medium voltage high power DC/DC converters for offshore wind energy systems," *IEEE Trans. Power Electron.*, vol. 28, no. 4, pp. 2014–2023, Apr. 2013.
[41] M. Zygmanowski, B. Grzesik, and R. Nalepa, "Capacitance and inductance selection of the modular multilevel converter," in *Proc. 15th Eur. Conf. Power Electron. Appl.*, Lille, France, 2013, pp. 1–10.
[42] Z. Liu, K. Li, J. Wang, Z. Javid, M. Wang, and K. Sun, "Research on capacitance selection for modular multi-level converter," *IEEE Trans. Power Electron.*, vol. 34, no. 9, pp. 8417–8434, Sep. 2019.
[43] M. Glinka, "Prototype of multiphase modular-multilevel-converter with 2 MW power rating and 17-level-output-voltage," in *Proc. IEEE 35th Annu. Power Electron. Specialists Conf.*, Aachen, Germany, 2004, pp. 2572–2576.
[44] T. Westerweller *et al.*, *Trans Bay Cable World's First HVDC System Using Multilevel Voltage Sourced Converter*. Paris, France: CIGRE, 2010, B4_101_201.
[45] M. S. Diab, A. M. Massoud, S. Ahmed, and B. W. Williams, "A dual modular multilevel converter with high-frequency magnetic links between submodules for MV open-end stator winding machine drives," *IEEE Trans. Power Electron.*, vol. 33, no. 6, pp. 5142–5159, Jun. 2018.
[46] *ABB HiPak 5SNA 1200G450300*, 2020. [Online]. Available: https://search.abb.com/library/Download.aspx?DocumentID=5SYA%201401-04&LanguageCode=en&DocumentPartId=&Action=Launch
[47] *ABB HiPak 5SNA 0650J450300*, 2020. [Online]. Available: https://search.abb.com/library/Download.aspx?DocumentID=5SYA%201598-04&LanguageCode=en&DocumentPartId=&Action=Launch.
[48] Y. Zhu and X. Lu, "Thermal-resistance calculation of the forced air cooling heatsink applying for power semiconductor devices," *Power Electron.*, vol. 3, no. 6, pp. 47–51, 2009.
[49] M. Leibl, G. Ortiz, and J. W. Kolar, "Design and experimental analysis of a medium-frequency transformer for solid-state transformer applications," *IEEE J. Emerg. Sel. Topics Power Electron.*, vol. 5, no. 1, pp. 110–123, Mar. 2017.
[50] G. Ortiz, M. Leibl, J. W. Kolar, and O. Apeldoorn, "Medium frequency transformers for solid-state-transformer applications—Design and experimental verification," in *Proc. Int. Conf. Power Electron. Drive Syst.*, Kitakyushu, Japan, 2013, pp. 1285–1290.
[51] W. G. Hurley and W. H. Wölfle, *Transformers and Inductors for Power Electronics: Theory, Design and Applications*. 1st ed. Hoboken, NJ, USA: Wiley, 2013.
[52] T. Nakanishi, "High power density design for a modular multilevel converter with an H-bridge cell based on a volume evaluation of each component," *IEEE Trans. Power Electron.*, vol. 33, no. 3, pp. 1967–1984, Mar. 2018.
[53] Z. Wang, Y. Zhang, H. Wang, and F. Blaabjerg, "A reference submodule based capacitor condition monitoring method for modular multilevel converters," *IEEE Trans. Power Electron.*, vol. 35, no. 7, pp. 6691–6696, Jul. 2020.
[54] Nichicon capacitors. 2020. [Online]. Available: https://cn-nichicon.com/products/pdfs/c-lnx.pdf
[55] TDK capacitors. 2020. [Online]. Available: https://www.tdk-electronics.tdk.com/inf/20/50/ds/MKP_DC_B2568X_ed2.pdf

Jiaxun Teng received the B.S. degree in electrical engineering from the Harbin Institute of Technology, Weihai, China, in 2017. He is currently working toward the M.S. degree in power electronics with Yanshan University, Qinhuangdao, China.

His current research interests include circuit topology, analysis and control of modular multilevel converter-based medium and high-voltage direct current systems, multiple-input power router, and power electronics transformer.

Xiaofeng Sun (Member, IEEE) received the B.S. degree in electrical engineering from Northeast Heavy Machinery Institute, Heilongjiang, China, in 1993, and the M.S. and Ph.D. degrees in power electronics from Yanshan University, Qinhuangdao, China, in 1999 and 2005, respectively.

From 2003 to 2007, he was an Associate Professor with Yanshan University, where he has been a Professor since 2008. He is also the Director with the Key Laboratory of Power Electronics for Energy Conservation and Motor Drive of Hebei Province. He has authored or coauthored more than 70 transactions and conference papers. His research interests include dc–dc converters, multiple-input converters, hybrid electric vehicles, microgrids, and power quality control.

Zemin Bu received the B.S. degree in electrical engineering from the Shanxi Institute of Technology, Yangquan, China, in 2018. He is currently working toward the Ph.D. degree in electrical engineering with Yanshan University, Qinhuangdao, China.

His current research interests include modular multilevel converter and solid state transformer.

Wei Zhao received the B.S. and M.S. degrees in electrical engineering and power electronics and power drives and the Ph.D. degree in power electronics from Yanshan University, Qinhuangdao, China, in 2006, 2009, and 2020, respectively.

His current research interests include the stability analysis of microgrid and power quality.

Xin Li received the B.Eng. degree in computer software and applications from Northeast Heavy Machinery College, Yanshan University, Qinhuangdao, China, in 1992, and the M.Eng. degree in measurement technique and automation equipment and the Ph.D. degree in measurement technology and instruments from Yanshan University, Qinhuangdao, China, in 2002 and 2008, respectively.

Her current research interests include power electronics, intelligent information processing, bioinformatics, and biomedical instruments.